NEUTRON STAR ENVELOPES AND THERMAL RADIATION FROM THE MAGNETIC SURFACE

JOSEPH VENTURA
Physics Department, University of Crete, and IESL, FORTH
71003 Heraklion, Crete, Greece

AND

ALEXANDER Y. POTEKHIN
Ioffe Physico-Technical Institute, 194021 St.Petersburg, Russia

Abstract. The thermal structure of neutron star envelopes is discussed with emphasis on analytic results. Recent progress on the effect of chemical constitution and high magnetic fields on the opacities and the thermal structure is further reviewed in view of the application to pulsar cooling and magnetars.

1. Introduction

Neutron stars (NS) are formed with very high internal temperatures approaching 10^{11} K in the core of a supernova explosion (see, e.g., Shapiro & Teukolski 1983 – ST83 in the following). Copious neutrino emission brings the temperature in the stellar core down to $\simeq 10^9$ K within about one day and then, more gradually, to $\simeq 10^8$ K within 10^4 years. It was realized early on that such objects were likely to have effective surface temperatures of the order of 10^6 K (Chiu & Salpeter 1964). Comparison with theoretical cooling curves can further provide information on aspects of the internal structure of NS such as superfluidity and the possible appearance of pion or kaon condensates and strange matter in their interior (e.g., Pethick 1992; Page 1997; Tsuruta 1998). It is then clear that the observation of this surface cooling X-ray emission is an objective of prime scientific importance.

The observation of such faint point sources has turned out to be difficult however, having to await the modern era of imaging X-ray telescopes. *ROSAT* observations in the 90's finally yielded improved spectral information, opening a new chapter in our ability to probe the internal structure

of superdense matter. Joachim Trümper (this meeting) already gave us an overview of the recent observations in this field (see also Caraveo *et al.* 1996; Trümper & Becker 1997). Increasing interest is also presently being directed on the new and important subject of magnetars, extensively discussed during this meeting.

Theoretical models of NS cooling are of necessity rather complicated, requiring detailed understanding of the stellar structure, equation of state (EOS), and thermal balance over an enormous range of densities and chemical diversity (e.g., Pethick 1992; Tsuruta 1998, and references therein). During an initial period of $10^5 - 10^6$ y the star cools principally via neutrino emission from its interior. There are many neutrino emission mechanisms, whose rates depend on the state of matter, particularly on nucleon superfluidity (for a review see Yakovlev *et al.* 1999). An older NS cools mainly via photon emission from its surface. Finally, the cooling may also be influenced by heating processes such as friction due to differential rotation between the superfluid and normal parts of the star (e.g., Alpar *et al.* 1989), β-processes arising from chemical imbalance during the spindown (Reisenegger 1997), and pulsar polar cap heating due to impinging charged particles accelerated in the magnetosphere (e.g., Halpern & Ruderman 1993).

Analysis of the NS thermal evolution is considerably simplified however by the fact that the stellar interior, from densities of $\simeq 10^{10}$ g cm^{-3} inward, is nearly isothermal because of the very high thermal conductivity in these layers. It is therefore convenient to establish a relation between this interior temperature $T_{\rm i}$, defined as the temperature at mass density $\rho = 10^{10}$ g cm^{-3}, and the effective surface temperature $T_{\rm e}$ (Gudmundsson *et al.* 1983 – GPE in the following). Thus, it becomes possible to examine separately the properties and structure of the outer envelope, which turns out to be crucial in determining the ratio $T_{\rm e}/T_{\rm i}$ and the nature of the emitted radiation (e.g., GPE; Hernquist & Applegate 1984 – HA84 in the following; Ventura 1989; Potekhin *et al.* 1997 – PCY in the following).

In the next section, we consider basic features of the mechanical and thermal structure of the outer NS envelope without magnetic field. The strong magnetic field ($B \gg 10^{10}$ G), which was found in most of the pulsars, shifts the atmosphere bottom and the region of partial ionization to higher densities. Furthermore, it strongly affects the radiative and thermal transport through the envelope. These effects will be discussed in Sect. 3.

2. Outer Envelope of a Neutron Star

The *outer envelope* consists mainly of electrons and ions. It extends down to a depth of a few hundred meters, where the density 4.3×10^{11} g cm^{-3} is reached. At this density, neutrons begin to drip from the nuclei (e.g.,

ST83). Thus the *inner envelope*, which extends deeper down to the core, consists of electrons, atomic nuclei, and free neutrons.

The outer envelope can be divided into the atmosphere, the liquid ocean, and the solid crust. The outermost layer constitutes a thin (0.1 – 100 cm) NS atmosphere (optical depth $\tau \lesssim 1$), where the outgoing radiation is formed. The plasma density at the atmosphere bottom is about 0.001 – 0.1 g cm^{-3}, depending on temperature, surface gravity, and chemical composition. This plasma can be partially ionized and non-ideal. Bound species can be distinct until the electron Fermi energy becomes comparable with the Thomas–Fermi energy at $\rho \lesssim 10\,ZA$ g cm^{-3}, A and Z being the mass and charge numbers. At higher densities the ions are immersed in a jellium of degenerate electrons, which still strongly responds to the Coulomb fields of the ions as long as $\rho \lesssim 10\,Z^2A$ g cm^{-3}.

In the rest of the envelope (at $\rho \gg 10\,Z^2A$ g cm^{-3}) the electrons form a strongly degenerate, almost ideal gas. This gas is non-relativistic at $\rho_6 \ll 1$ and ultrarelativistic at $\rho_6 \gg 1$, where $\rho_6 \equiv \rho/10^6$ g cm^{-3}. The ions form a Coulomb gas or liquid at $\Gamma \lesssim 175$, where $\Gamma \approx 22.75\,(\rho_6/\mu_{\rm e})^{1/3}\,Z^{5/3}/T_6$ is the Coulomb coupling parameter, $T_6 = T/10^6$ K, $\mu_{\rm e} = A/Z$. At $\Gamma \approx 175$, the liquid freezes into a Coulomb crystal. The pressure is almost entirely determined by degenerate electrons and thus independent of T, while the mass density is mostly determined by the ions.

While cooling of the NS during the initial neutrino dominated era is not influenced by the outer layers, it is in fact the properties of these surface layers that characterize the flux and photon spectrum emitted at the NS surface, leading in turn to estimates of $T_{\rm i}^{\infty}$. At the subsequent photon cooling stage, the heat insulation by the envelope controls the cooling rate. The radiation is reprocessed in the atmosphere, which yields an emitted spectrum, in general different from that of a black body (Romani 1987). The properties of these layers are thus crucial to interpreting observations and, understandably, a lot of theoretical work has been devoted to analyzing the thermal structure of non-magnetic and magnetic NS envelopes (e.g., GPE; PCY; Heyl & Hernquist 1998) and the radiation properties of their atmospheres (e.g., Pavlov *et al.* 1995; Page & Sarmiento 1996; Rajagopal *et al.* 1997; Potekhin *et al.* 1998, and references therein).

2.1. MECHANICAL STRUCTURE

To review the cardinal properties of the NS surface layers, let us recall the enormous gravitational potential $GM/R \approx 0.148\,(M/M_\odot)\,R_6^{-1}\,c^2$ (where $R_6 \equiv R/10^6$ cm ~ 1 and $M/M_\odot \simeq 1.4$ for most typical NS), which renders effects of General Relativity appreciable. Indeed, the Schwarzschild radius $r_g = 2GM/c^2 \approx 2.95\,(M/M_\odot)$ km is not much smaller than the stellar

radius R (throughout this review, M is the gravitational mass of the star, which is 10–15% smaller than its baryon mass). The hydrostatic equilibrium is then governed by the Oppenheimer–Volkoff equation (e.g., Thorne 1977). Introducing the local proper depth $z = (R - r)\,(1 - r_g/R)^{-1/2}$ (where r is the radius), in the surface layers ($z \ll R$) one can rewrite this equation in the Newtonian form

$$\mathrm{d}P/\mathrm{d}z = g\rho, \tag{1}$$

where

$$g = \frac{GM}{R^2\,(1 - r_g/R)^{1/2}} \approx 1.327 \times 10^{14}\,(1 - r_g/R)^{-1/2}\,\frac{M}{M_\odot}\,R_6^{-2}\ \mathrm{cm\ s^{-2}}$$

is the local gravitational acceleration at the surface.

Since the surface gravity is huge, the atmosphere's scale height is rather small. In the non-degenerate layers, we have

$$P = (\rho/\mu m_\mathrm{u})\,kT, \tag{2}$$

where $m_\mathrm{u} = 1.6605 \times 10^{-24}$ g is the atomic mass unit and $\mu = A/(Z + 1)$. Thus, following a thin non-degenerate atmosphere of a scale height $P/(g\rho) \approx 0.626\,(T_6/\mu)\,R_6^2\,(M/M_\odot)^{-1}$ cm, electron degeneracy sets in at densities $\rho \gtrsim 6\,\mu_\mathrm{e} T_6^{3/2}$ g cm^{-3}.

The electron kinetic energy at the Fermi surface is $kT_\mathrm{F} \equiv \epsilon_\mathrm{F} - m_\mathrm{e}c^2$, where k is the Boltzmann constant,

$$T_\mathrm{F} = (\gamma_\mathrm{F} - 1)\,m_\mathrm{e}c^2/k = 5.93 \times 10^9\ \chi^2/(1 + \gamma_\mathrm{F})\ \mathrm{K} \tag{3}$$

is the Fermi temperature, and

$$\gamma_\mathrm{F} = \sqrt{1 + \chi^2}, \qquad \chi = \frac{p_\mathrm{F}}{m_\mathrm{e}c} = \frac{\hbar(3\pi^2 n_\mathrm{e})^{1/3}}{m_\mathrm{e}c} \approx 1.009\left(\frac{\rho_6}{\mu_\mathrm{e}}\right)^{1/3}, \tag{4}$$

are the electron Lorentz factor and *relativity parameter*, respectively.

Elementary fitting formulae to the pressure of fully ionized ion-electron plasmas as function of density at arbitrary electron degeneracy and temperature have been presented by Chabrier & Potekhin (1998). These formulae can also be extended to partially ionized atmospheric layers in the mean-ion approximation, provided the effective ion charge Z is known (cf. PCY). At sufficiently high density, however, where $T_\mathrm{F} \gg T$, the main contribution is that of strongly degenerate electrons with the pressure depending only on the density through the parameter χ (e.g., ST83):

$$P_\mathrm{e} = \frac{P_0}{8\pi^2}\left[\chi\left(\frac{2}{3}\,\chi^2 - 1\right)\gamma_\mathrm{F} + \ln(\chi + \gamma_\mathrm{F})\right] \tag{5}$$

where $P_0 \equiv m_{\rm e}c^2/\lambda\!\!\!^{-3} = 1.4218 \times 10^{25}$ dynes cm^{-2} is the relativistic unit of pressure, $\lambda\!\!\!^{-} = \hbar/(m_{\rm e}c)$ being the Compton wavelength. This may further be approximated as $P_{\rm e} \approx P_0 \chi^{3\gamma_{\rm ad}}/(9\pi^2\gamma_{\rm ad})$, where $\gamma_{\rm ad}$ is the adiabatic index, equal to 5/3 at $\chi \ll 1$ and 4/3 at $\chi \gg 1$.

Note that for strongly degenerate electrons

$$\mathrm{d}P = n_{\rm e}\,\mathrm{d}\epsilon_{\rm F} = 4.93 \times 10^{17}\ \mathrm{erg\ g^{-1}}\,(\rho/\mu_{\rm e})\,\chi\,\mathrm{d}\chi/\gamma_{\rm F}. \tag{6}$$

From Eqs. (1) and (6), one obtains

$$1.027\,\frac{\rho_6}{\mu_{\rm e}} = \chi^3 = \left[\frac{z}{z_0}\left(2+\frac{z}{z_0}\right)\right]^{3/2}, \quad z_0 = \frac{m_{\rm e}c^2}{m_{\rm u}g\mu_{\rm e}} \approx \frac{4930\ \mathrm{cm}}{\mu_{\rm e}\,g_{14}}, \tag{7}$$

where $g_{14} = g/(10^{14}\ \mathrm{cm\,s^{-2}})$, and z_0 is a depth scale at which degenerate electrons become relativistic.

Let us note also that the mass ΔM contained in a layer from the surface to a given depth z is solely determined by the pressure $P(z)$ at the bottom of the given layer:

$$\Delta M(z) = 4\pi R^2\,P(z)\,g^{-1}\,(1-r_g/R)^{1/2} \approx 1.192\times10^{-9}\,g_{14}^{-2}\,MP(z)/P_0. \tag{8}$$

2.2. THERMAL STRUCTURE

From Eqs. (7) and (8), we see that the outer envelope is a very thin layer – typically within the outer 100 m, containing $\sim 10^{-7}\mathrm{M}_\odot$, – which renders the thermal diffusion problem essentially plane-parallel and one-dimensional. Assuming a constant heat flux throughout the outer envelope, the temperature profile can be obtained by solving the heat diffusion equation:

$$F = \kappa\frac{\mathrm{d}T}{\mathrm{d}z} = \frac{16\sigma}{3}\frac{T^3\,\mathrm{d}T}{\mathrm{d}\tau}, \quad \kappa \equiv \frac{16\sigma T^3}{3K\rho}, \tag{9}$$

where F is the heat flux, κ is thermal conductivity, σ is the Stefan–Boltzmann constant, and K is the usual Rosseland mean over the energy spectrum of the specific opacity. This leads immediately to a temperature profile $T/T_{\rm e} \approx (\frac{3}{4}\tau + \frac{1}{2})^{1/4}$, where the *local* effective surface temperature $T_{\rm e}$ is defined through $F = \sigma T_{\rm e}^4$ and the integration constant corresponds to the Eddington approximation ($\tau = \frac{2}{3}$ at the *radiative surface*, where $T = T_{\rm e}$). A more accurate boundary condition requires solution of the radiative transfer equation in the atmosphere. A distant observer would infer from the spectrum and flux the redshifted surface temperature $T_\infty = T_{\rm e}\,(1 - r_g/R)^{1/2}$ and apparent radius $R_\infty = R\,(1 - r_g/R)^{-1/2}$ (e.g., Thorne 1977).

A knowledge of the mean opacity $K(\rho, T)$ is then needed to relate the temperature to the other plasma parameters, which can then also be expressed as functions of the optical depth τ. It is also needed in order to compute the overall depth and the temperature ratio $T_{\rm i}/T_{\rm e}$.

2.2.1. *Opacity*

Heat is transported through the envelope mainly by radiation and by conduction electrons. In general, the two mechanisms work in parallel, hence

$$\overline{\kappa} = \kappa_{\rm r} + \kappa_{\rm c}, \qquad K^{-1} = K_{\rm r}^{-1} + K_{\rm c}^{-1}, \tag{10}$$

where $\kappa_{\rm r}$, $\kappa_{\rm c}$ and $K_{\rm r}$, $K_{\rm c}$ denote the radiation and conduction components of the conductivity and opacity, respectively. Typically, the radiative conduction dominates the thermal transport ($\kappa_{\rm r} > \kappa_{\rm c}$) in the outermost non-degenerate layers of a NS, whereas electron conduction dominates ($\kappa_{\rm c} > \kappa_{\rm r}$) in deeper, mostly degenerate layers. In the absence of intense magnetic fields, modern cooling calculations (e.g., PCY) make use of the Livermore library of radiative opacities OPAL (Iglesias & Rogers 1996), which also provides an EOS for the relevant thermodynamic parameters at $\rho \lesssim 10\, T_6^3$ g cm^{-3}. For the electron conduction regime, modern opacities have been worked out by Potekhin *et al.* (1999a).

Radiative opacities. In order to derive an analytic model of the NS envelope, HA84 and Ventura (1989) have written the atmospheric opacity in the form

$$K(\rho, T) = K_0 \rho^{\alpha}\, T^{\beta}. \tag{11}$$

In particular, this relation describes the opacity given by the Kramers formula, which corresponds to $\alpha = 1$ and $\beta = -3.5$. In a fully ionized, non-relativistic and non-degenerate plasma, the opacity provided by the free-free transitions is (e.g., Cox & Giuli 1968)

$$K_{\rm r} \approx 75\, \bar{g}_{\rm eff}\, (Z/\mu_{\rm e}^2)\, \rho\, T_6^{-3.5}\ {\rm cm}^2/{\rm g}, \tag{12}$$

where ρ is in g cm^{-3} and $\bar{g}_{\rm eff} \sim 1$ is an effective dimensionless Gaunt factor, a slow function of the plasma parameters. For a colder plasma, where bound-free transitions dominate over free-free ones, the Kramers formula remains approximately valid, but the opacity K is about two orders of magnitude higher. An order-of-magnitude (within ≈ 0.5 in $\log K$) approximation to the realistic OPAL opacities for hydrogen in the range of parameters $T_6 \sim 10^{-1} - 10^{0.5}$ and $\rho \sim (10^{-2} - 10^{1})\, T_6^3$ is given by Eq. (12) if we put formally $\bar{g}_{\rm eff} \approx \rho^{-0.2}$. An analogous order-of-magnitude approximation to the OPAL opacities for iron at $T_6 \sim 10^{0} - 10^{1.5}$ and $\rho \sim (10^{-4} - 10^{-1})\, T_6^3$ is obtained with $\bar{g}_{\rm eff} \approx 70\, \rho^{-0.2}$. These approximations also belong to the class of functions (11), but with $\alpha = 0.8$.

Conductive opacities. Thermal conduction of degenerate matter in deeper layers is dominated by electrons which scatter off ions. This conductivity can be written as (Yakovlev & Urpin 1980)

$$\kappa_{\rm c} = \frac{\pi k^2 T m_{\rm e} c^3 \chi^3}{12 Z e^4 \Lambda \gamma_{\rm F}^2} \approx 2.3\times10^{15}\,\frac{T_6}{\Lambda Z}\,\frac{\chi^3}{1+\chi^2}\,\frac{\rm erg}{\rm cm\ s\ K}, \qquad (13)$$

where Λ is the Coulomb logarithm. Accurate analytic fitting formulas to Λ as function of ρ and T have been obtained recently by Potekhin *et al.* (1999a). In the solid crust, this function is reduced to small values by quantum and correlation effects in Coulomb crystals. However, we shall see shortly that in not too cold NS, the thermal profile is mainly formed in the liquid layers of the envelope. Therefore, for our purpose, it will be sufficient to note that in the NS ocean Λ is a slow function of the plasma parameters and can be approximated by a constant of the order of unity.

In the case of non-degenerate electrons, the conductivity can be found, e.g., by the method of Braginskiĭ (1957), which yields

$$\kappa_{\rm c}^{\rm nd} \approx 5\times10^{10}\,(F_Z/\Lambda)\,Z^{-1}\,T_6^{5/2}\ {\rm erg/(cm\ s\ K)}, \qquad (14)$$

where F_Z is a slow function of Z: for example, $F_{26} = 1.34$ and $F_1 = 0.36$, whereas the Coulomb logarithm Λ is ~ 1 near the onset of degeneracy and logarithmically increases with decreasing density. Effectively, Eq. (14) may be viewed as an analog to Eq. (13) where the dimensionless Fermi momentum χ has been replaced by an appropriate thermal average ($\propto\sqrt{T}$).

2.2.2. *Temperature Profile*

The simple functional form of the opacity allows now an analytic treatment of the thermal structure (Urpin & Yakovlev 1980; HA84; Ventura 1989).

Non-degenerate regime. Using Eqs. (1), (11), and (2) one may rewrite Eq. (9) as

$${\rm d}P = \frac{\kappa\, g\, \rho}{F}\,{\rm d}T = \frac{16}{3}\,\frac{g}{K}\,\frac{T^3\,{\rm d}T}{T_{\rm e}^4} = \frac{16}{3}\,\frac{g}{K_0}\left(\frac{k}{\mu m_{\rm u}}\right)^{\alpha}\frac{T^{3+\alpha-\beta}}{P^{\alpha}}\,\frac{{\rm d}T}{T_{\rm e}^4}, \qquad (15)$$

which is readily integrated from the surface inward to give the temperature profile. In the region far from the surface, where $T \gg T_{\rm e}$, the integration constants may be dropped. Using again Eqs. (2), one can present the result as a simple power law:

$$\frac{T^{3-\beta}}{\rho^{\alpha+1}} = \frac{3}{16}\,\frac{4+\alpha-\beta}{\alpha+1}\,\frac{k}{\mu m_{\rm u}}\,\frac{K_0 T_{\rm e}^4}{g}. \qquad (16)$$

This result depends on our implicit assumption that the effective ion charge Z remains constant, which in general is not strictly valid.

Interestingly enough, as noted by HA84, Eq. (16) establishes that the conductivity κ is constant throughout the radiative non-degenerate layer:

$$\kappa = \frac{16}{3}\frac{\sigma T^3}{K\rho} = \frac{16}{3}\frac{\sigma}{K_0}\frac{T^{3-\beta}}{\rho^{\alpha+1}} = \frac{4+\alpha-\beta}{1+\alpha}\frac{k\sigma T_{\rm e}^4}{\mu m_{\rm u} g}. \tag{17}$$

The constant value depends on the emitted flux, but is independent of K_0. It follows immediately from Eq. (9) that temperature grows linearly with geometrical depth. Furthermore, from Eq. (16) we obtain the T, ρ profile. In particular, substituting $\alpha = 1$ and $\beta = -3.5$, we obtain

$$K\rho = \frac{1.51}{\rm cm}\,\frac{\mu g_{14}}{T_{\rm e6}}\left(\frac{T}{T_{\rm e}}\right)^3, \quad \kappa = 2\times 10^{14}\,\frac{T_{\rm e6}^4}{\mu g_{14}}\,\frac{\rm erg}{\rm cm\,s\,K}. \tag{18}$$

Substitution of K from Eq. (12) yields

$$T_6 \approx 0.284\, g_{14}\,\mu\, z \approx (50\,\bar{g}_{\rm eff}\,q)^{2/13}\,(\rho/\mu_{\rm e})^{4/13}, \quad q \equiv T_{\rm e6}^4\, Z/(\mu g_{14}). \tag{19}$$

In these relations, z and ρ are measured in CGS units, and $T_{\rm e6} = T_{\rm e}/10^6$ K.

Radiative surface. It is further interesting to note that the opacity K is also slowly varying in this region. Combining Eqs. (11), and (19), we obtain $K \propto \rho/T^{3.5} \propto \rho^{-1/13}$. Invoking Eq. (2), we get $K \propto P^{-1/17}$. This justifies the assumption $K_{\rm r} \approx$ const, which one often employs when determining the radiative surface from equation (e.g., GPE; PCY)

$$(K_{\rm r} P)_{\rm surface} = (2/3)\, g. \tag{20}$$

Using Eqs. (2) and (12), we obtain

$$\rho_{\rm s} \approx 0.1\,\mu_{\rm e}\left(\frac{\mu}{Z\,\bar{g}_{\rm eff}}\,g_{14}\right)^{1/2} T_{\rm e6}^{5/4}\ {\rm g\,cm^{-3}}. \tag{21}$$

Substituting $\bar{g}_{\rm eff} \simeq 1$ and $\bar{g}_{\rm eff} \simeq 200$ for hydrogen and iron, respectively, we obtain $\rho_{\rm s} \sim 0.07\sqrt{g_{14}}\,T_{\rm e6}^{5/4}$ g cm^{-3} and $\rho_{\rm s} \sim 0.004\sqrt{g_{14}}\,T_{\rm e6}^{5/4}$ g cm^{-3} for these two elements, in reasonable agreement with numerical results of PCY.

Onset of degeneracy. The solution given by Eq. (19) can be extended down to a depth where the electrons become degenerate. Let us estimate this depth from the condition $kT_{\rm d} = p_{\rm F}^2/2m_{\rm e}$. We obtain

$$\chi_{\rm d} \simeq 0.053\,(\bar{g}_{\rm eff}\,q)^{1/7}, \quad T_{\rm d} \simeq 8.5\times 10^6\,(\bar{g}_{\rm eff}\,q)^{2/7}\ {\rm K}. \tag{22}$$

Even for very high $T_{\rm e} \sim 10^7$ K, we have $\chi_{\rm d} \lesssim 1$, i.e. the electrons are non-relativistic at the degeneracy boundary. With decreasing $T_{\rm e}$, the quantities $\chi_{\rm d}$ and $T_{\rm d}$ decrease, i.e. the boundary shifts toward the stellar surface.

Sensitivity strip. Numerical cooling calculations (GPE) revealed early on that accurate knowledge of the opacity law is especially important within a certain "sensitivity strip" in the (ρ, T) plane. The temperature ratio $T_\mathrm{i}/T_\mathrm{e}$ changes appreciably if K is modified by, say, a factor 2 within this narrow strip, while comparable changes of K outside the strip would leave this ratio unaffected within a high degree of accuracy.

The importance of the layer in the outer envelope where the opacity (10) turns from radiative to conduction dominated is now easy to demonstrate. In the non-degenerate radiative part the integral over ρ is dominated by the higher densities near the base of the layer, while in the degenerate, conductive layer it is dominated by the top, least dense part of the layer. The region where K turns from radiative to conductive is thus seen to contribute most of the resistance to heat flow. The line in the (ρ, T) plane where $K_\mathrm{r} = K_\mathrm{c}$ is easily determined from Eqs. (12) and (13):

$$\rho \approx 12\,\mu_\mathrm{e}\bar{g}_\mathrm{eff}^{-1/3}\,T_6^{11/6}\ \mathrm{g\,cm^{-3}}. \tag{23}$$

On the right-hand side, we have approximated the factor $(\Lambda\gamma_\mathrm{F}^2)^{1/3}$ by unity. Using again the solution (16), we find explicitly the temperature T_t and relativity factor χ_t at the turning point from radiative to electron conduction:

$$T_\mathrm{t} \approx 2.3\times10^7\,\bar{g}_\mathrm{eff}^{2/17}\,q^{6/17}\ \mathrm{K}, \quad \chi_\mathrm{t} \approx 0.157\,\bar{g}_\mathrm{eff}^{-2/51}q^{11/51}. \tag{24}$$

Some caution is necessary here, however, because the approximation $K \simeq K_\mathrm{r}$ is not justified as we approach the turning point: actually, at this point $K = K_\mathrm{r}/2$, as seen from Eq. (10). In addition, the extrapolation of the solution (19) to the turning point is, strictly speaking, not justified, since the electron gas becomes degenerate: $\chi_\mathrm{t} > \chi_\mathrm{d}$ for most typical NS parameters. Nevertheless, since χ_t and χ_d are not very much different, the section of the thermal profile where our assumptions are violated is relatively small, so Eq. (24) provides a reasonable approximation. This is confirmed by a direct comparison with numerical results (PCY), which reveals an error within only a few tens percent, provided $T \gtrsim 10^{5.5}$ K.

Solution beyond the turning point. An analytic solution to the thermal profile in degenerate layers of a NS envelope has been first obtained by Urpin & Yakovlev (1980), based on the conductivity in the form (13). The hydrostatic equilibrium of the degenerate surface layers is determined by Eqs. (1) and (6), which yield $g m_\mathrm{u}\,\mu_\mathrm{e} = m_\mathrm{e}c^2(\chi/\gamma_\mathrm{F})\,\mathrm{d}\chi/\mathrm{d}z$. Using the heat diffusion equation (9) and Eq. (13), we obtain

$$T\frac{\mathrm{d}T}{\mathrm{d}\chi} = \frac{12}{\pi}\,\frac{FZe^4\Lambda}{m_\mathrm{u}k^2cg\mu_\mathrm{e}}\,\frac{\gamma_\mathrm{F}}{\chi^2} = (1.56\times10^7\ \mathrm{K})^2\,\frac{Z\Lambda T_{\mathrm{e}6}^4}{\mu_\mathrm{e}g_{14}}\,\frac{\gamma_\mathrm{F}}{2\chi^2}. \tag{25}$$

Treating Λ, A, and Z as constants, we can integrate this equation from $\chi_{\rm t}$ inwards and obtain

$$T^2(z) = T_{\rm t}^2 + (1.56\times10^7\ {\rm K})^2\,\frac{Z\Lambda T_{\rm e6}^4}{\mu_{\rm e} g_{14}}\,[f(\chi)-f(\chi_{\rm t})]\,, \qquad (26)$$

where $f(\chi)\equiv\ln(\chi+\gamma_{\rm F})-\gamma_{\rm F}/\chi$, and the dependence of χ on z is given by Eq. (7).

Let us use the above solution to evaluate $T_{\rm i}$. Since $\chi_{\rm t}\lesssim 1$, but $\chi\gg1$, it is easy to see that $[f(\chi)-f(\chi_{\rm t})]\approx\chi_{\rm t}^{-1}$ in Eq. (26). Using Eq. (24), we obtain

$$T_{\rm i} = \left(T_{\rm t}^2+T_\Delta^2\right)^{1/2}, \quad T_\Delta \approx 4\times10^7\left(\frac{Z\,T_{\rm e6}^4}{\mu_{\rm e}g_{14}}\right)^{20/51}\ {\rm K}, \qquad (27)$$

where we have neglected some factors which are close to unity.

Figure 1 illustrates the accuracy of the above analytic solution as well as its limitations. Here, solid lines show temperature profiles of a NS with mass $M=1.4\,M_\odot$ and radius $R=10$ km obtained by solving the radiative transfer equation with spectral OPAL opacities in the atmosphere and integrating the thermal structure equation (9) with accurate radiative and conductive Rosseland opacities inwards in the deeper layers (Shibanov *et al.* 1998). Dashed curves depict the above analytic approximations. The left panel corresponds to an envelope composed of iron, and the right panel shows the thermal structure of an accreted envelope with its outermost layers composed of hydrogen, which is further burnt into heavier elements (He, C, Fe) in deeper and hotter layers. This thermo- and pycnonuclear burning is responsible for the complex shape of the upper profile. Different straight lines show the points at which thermal profiles corresponding to various heat fluxes would cross the radiative surface, the region of the onset of degeneracy, turning points $K_{\rm c}=K_{\rm r}$, and (on the left panel) the bottom of the ocean. The latter line is not present on the right panel, because freezing of hydrogen and helium is suppressed by large zero-point ionic vibrations (cf. Chabrier 1993).

One can see that not only the above analytic approximations correctly describe the qualitative structure of the envelope, but they also provide a reasonable quantitative estimate of the temperature at a given density. The accuracy deteriorates for lower $T_{\rm e}$ (especially when Z is high), because in this case radiative opacities are affected by bound-bound transitions and strong plasma coupling effects and thus no longer obey the simple power law (12).

Discussion. We have seen that the internal temperature $T_{\rm i}$ is determined by two temperatures, $T_{\rm t}$ and T_Δ, related to the non-degenerate and de-

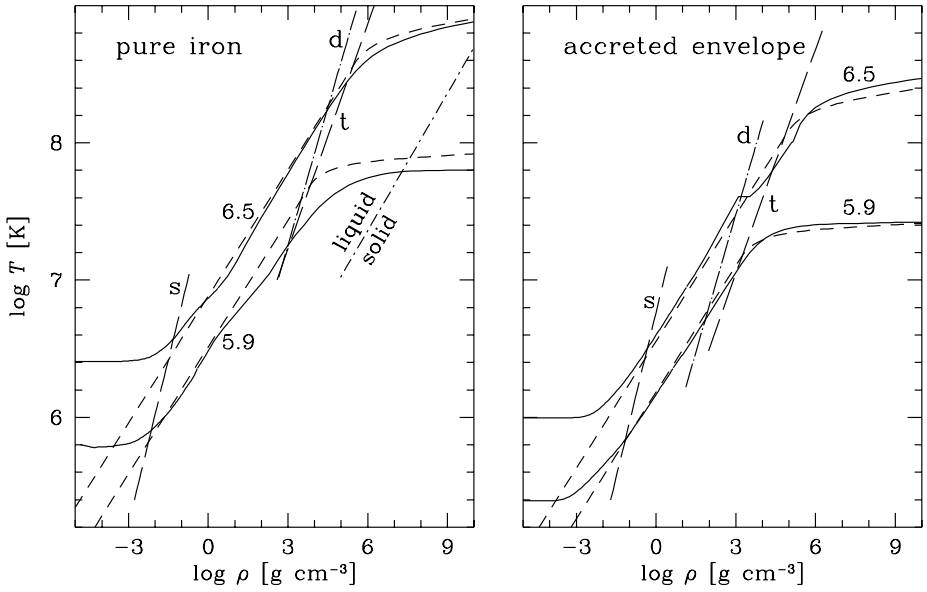

Figure 1. Thermal profiles inside non-accreted (left panel) and accreted (right panel) envelopes of NS at two effective temperatures, $\log T_{\rm e}$ [K] = 5.9 and 6.5 (marked near the curves). Solid curves – numerical solution (Shibanov *et al.* 1998), dashed curves – analytic approximations (19) and (27). Straight lines marked "s", "d," and "t" give the values ρ and T at which the various temperature profiles cross the radiative surface [Eq. (21)], the onset of electron degeneracy [Eq. (22)], and the turning point [Eq. (24)], respectively. The Fe melting line is also shown.

generate layers, respectively, and that the temperature growth occurs in the very surface layers of the star. This justifies the separation of the NS into a blanketing envelope and internal isothermal layers used in numerical simulations (GPE; PCY). We have also shown, in agreement with GPE, that the bulk of the envelope's thermal insulation arises in the relatively low density region around the turning point defined by Eq. (24).

The dependence on Z and $\mu_{\rm e}$ that enters Eqs. (27) makes the $T_{\rm i}/T_{\rm e}$ ratio sensitively dependent of the chemical composition of the envelope. If we replace the iron envelope by an accreted envelope composed of hydrogen or helium, we get this ratio reduced by about a half order of magnitude, which corresponds to two orders of magnitude higher photon luminosity at a given internal temperature. Thus an envelope composed of light elements is much more transparent to heat, and this strongly affects cooling, as noted by PCY. Our analytic estimates present a tool for the fast estimation of the magnitude of such effects.

In the next section we will see how these principal properties change as a result of a strong magnetic field permeating the NS envelope.

3. Effects of Magnetic Fields

It is well known that the strong magnetic field can profoundly alter the physical properties of the NS outer layers – for reviews see Canuto & Ventura (1977), Mészáros (1992), and Yakovlev & Kaminker (1994). We will be interested here in modifications introduced by the intense field B in the EOS, the Fermi temperature $T_{\rm F}$, and the opacity K, all of which affect the heat transfer problem. Our primary focus will be on the properties of an electron gas. Free ions give only a minor contribution to the opacities, whereas their contribution to the EOS remains unaffected by the field in the non-degenerate regime and is negligible when electrons are strongly degenerate.

Apart from the bulk properties of the electron plasma, magnetic fields also modify profoundly the properties of atoms which become very elongated and compact, having sharply increased binding energies (e.g., Canuto & Ventura 1977). This should strongly affect the emitted spectra from NS surfaces. Many works have been devoted in the past to the calculation of quantum-mechanical properties of atoms at rest in strong magnetic fields (e.g., Miller & Neuhauser 1991). Some of them have been used to construct magnetic NS atmosphere models (Rajagopal *et al.* 1997). However, thermal motion of the atoms at realistic NS temperatures breaks down the axial symmetry and may completely alter atomic properties. It is therefore necessary to have quantum-mechanical calculations for *moving* atoms, and their results should be included in models of EOS and opacities. Such models are available to date only for hydrogen (e.g., Potekhin *et al.* 1998, 1999b, and references therein). For other species, this work still remains to be done.

In the past, a lot of work has also been devoted to evaluating the conditions under which magnetic molecular chains may become stable in the surface layers; furthermore, in superstrong fields they may form a magnetically stabilized lattice (e.g., Ruderman 1971; Lai & Salpeter 1997). Such a phase transition is also expected to have observable consequences, but the field still remains largely unexplored.

3.1. ELECTRON GAS IN MAGNETIC FIELD

Motion of free electrons perpendicular to the magnetic field is quantized in Landau orbitals with a characteristic transverse scale equal to the *magnetic length* $a_{\rm m} = (\hbar c/eB)^{1/2} = \lambda\!\!\!^{-}/\sqrt{b}$, where $b = \hbar\omega_{\rm c}/m_e c^2 = B_{12}/44.14$ is the magnetic field strength expressed in relativistic units, $\omega_{\rm c} = eB/mc$ is the electron cyclotron frequency, and $B_{12} \equiv B/10^{12}$ G. The Landau energy

levels are

$$\epsilon = \epsilon_n(p_z) = c\left(m_e^2c^2 + 2\hbar\omega_c m_e n + p_z^2\right)^{1/2}, \tag{28}$$

with $n = 0, 1, 2, ...$, where the magnetic field $\boldsymbol{B}$ is assumed to be homogeneous and directed along the z axis, and p_z is the longitudinal momentum. The ground Landau level $n = 0$ is non-degenerate with respect to spin projection ($s = -1$, statistical weight $g_0 = 1$) while the levels $n > 0$ are doubly degenerate ($s = \pm 1$, $g_n = 2$). The anomalous magnetic moment of the electron, $g_e = 1.00116$, causes splitting of the energy levels $n \geq 1$ by $\delta\epsilon = (g_e - 1)\hbar\omega_c$, which, strictly speaking, removes the double spin-degeneracy. In typical NS envelopes, this splitting is negligible because $\delta\epsilon$ is smaller than either the thermal width $\sim kT$ or the collisional width of the Landau levels.

The electron's phase space is thus now a combination of an energy continuum in p_z, corresponding to the motion along the field, and a discrete spectrum (the quantum number n) corresponding to the quantized transverse motion. This property will be reflected in most of the physical processes of our interest here.

Let us denote by n^* the highest Landau excitation populated at a given energy ϵ. It equals an integer part of the combination $p_0^2(\epsilon)/(2m_e\hbar\omega_c)$, where $p_n(\epsilon) = [(\epsilon/c)^2 - (m_e c)^2 - 2m_e\hbar\omega_c n]^{1/2} = |p_z|$. Taking into account that the number of quantum states of an electron with given s and n in volume V per longitudinal momentum interval Δp_z equals $V\Delta p_z/(4\pi^2 a_m^2\hbar)$, one can obtain the electron number density and pressure from first principles (e.g., Blandford & Hernquist 1982). For strongly degenerate electrons,

$$n_e = \frac{1}{2\pi^2 a_m^2\hbar}\sum_{n=0}^{n^*} g_n p_n(\epsilon_F), \tag{29}$$

$$P_e = P_0\,\frac{b}{4\pi^2}\sum_{n=0}^{n^*} g_n\,(1+2bn)\,[x_n\sqrt{1+x_n^2} - \ln(x_n + \sqrt{1+x_n^2})], \tag{30}$$

where $x_n = cp_n(\epsilon_F)/\epsilon_n(0)$, and P_0 is the same as in Eq. (5).

For a degenerate electron gas the thermodynamic quantities such as pressure, magnetization, and energy density exhibit quantum oscillations of the de Haas–van Alphen type whenever the dimensionless Fermi momentum reaches the characteristic values $\chi = \sqrt{2nb}$ which signify the occupation of new Landau levels. In these oscillations the various quantities typically take values around their classical $B = 0$ values, except in the limit of a *strongly quantizing* field ($n^* = 0$) where one often finds substantial deviations (e.g., Yakovlev & Kaminker 1994). The latter case takes place when the typical energies kT, $kT_F < \epsilon_1 - 1$ – i.e., at $T \ll T_B$ and $\rho < \rho_B$, where

$$\rho_B = m_u n_B \mu_e \approx 7045\, B_{12}^{3/2}\,\mu_e\ \mathrm{g\,cm^{-3}}, \tag{31}$$

$$T_B = \hbar\omega_c/k\gamma_{\rm F} \approx 1.343\times10^8\,(B_{12}/\gamma_{\rm F})\ {\rm K}, \quad (32)$$

and $n_B = 1/(\pi^2\sqrt{2}\,a_{\rm m}^3)$ is the electron number density at which the Fermi energy reaches the first excited Landau level. This case is of special interest for the NS outer layers under consideration.

Strongly quantizing field. When the electron's transverse motion is frozen in the ground state Landau level $n^* = 0$, the phase-space is effectively one-dimensional. Then $\epsilon = c\sqrt{(m_e c)^2 + p_z^2}$, and Eq. (29) simplifies to

$$p_{\rm F}/\hbar = 2\pi^2 a_m^2 n_{\rm e}. \quad (33)$$

We therefore see that the dimensionless Fermi momentum,

$$\chi \equiv p_{\rm F}/m_e c = (2/3)\,\chi_0^3/b \approx (0.6846/b)\,\rho_6/\mu_{\rm e}, \quad (34)$$

is proportional to the density ρ, in sharp contrast to the non-magnetic Eq. (4). Henceforth we denote $p_{\rm F0} = m_{\rm e}c\chi_0$ the "classical" (non-magnetic) Fermi momentum at a given density, and reserve notation $p_{\rm F} = m_{\rm e}c\chi$ for the same quantity modified by the magnetic field. According to Eq. (31), the strongly quantizing regime in which Eq. (34) is valid requires $\chi < \sqrt{2b}$.

The Fermi temperature $T_{\rm F}$ is again given by Eq. (3), but with the modified χ. Since $\chi = (4/3)^{1/3}(\rho/\rho_B)^{2/3}\chi_0$, $T_{\rm F}$ is strongly reduced at $\rho \ll \rho_B$. Conversely, at a given $T < T_B$, the degeneracy takes hold at much higher density than in the $B = 0$ case. An initially degenerate electron gas at $B = 0$ will thus become non-degenerate when a strong quantizing field is switched on.

Let us now consider the EOS. Since $n = 0$, Eq. (30) simplifies considerably. Given Eq. (34), this expression again takes the form of a power-law of the density, $P = P_0 b\chi^{\gamma_{\rm ad}}/(2\pi^2\gamma_{\rm ad}) \propto \rho^{\gamma_{\rm ad}}/B^{\gamma_{\rm ad}-1}$, with $\gamma_{\rm ad} = 3$ or 2 in the non-relativistic and ultrarelativistic limits, respectively.

3.2. MAGNETIC OPACITIES

In the presence of a magnetic field, the conductivity κ becomes a tensor, so that the heat fluxes along and across the field become different. Since the field varies over the NS surface, the heat transport becomes two-dimensional. Fortunately, since the crust thickness is relatively small, the one-dimensional equation (9) remains a good approximation, with $\kappa = \kappa_\parallel \cos^2\theta + \kappa_\perp \sin^2\theta$, where $\kappa_\parallel$ and $\kappa_\perp$ are the conductivities along and across $\boldsymbol{B}$ and θ is the angle between $\boldsymbol{B}$ and the normal to the surface.

Radiative opacities. In a magnetized plasma, two propagating polarization normal modes are defined in the presence of an external field having widely different mean free paths each in the various photon-electron interactions (e.g., Mészáros 1992; Pavlov *et al.* 1995). Silant'ev & Yakovlev (1980) have calculated the Rosseland opacities for the cases when they are determined by the Thomson and free-free processes. When $T_B \gg T$, $\kappa_{\rm r}$ grows proportionally to $(T_B/T)^2$ – i.e., $K_{\rm r}$ decreases as $(T/T_B)^2$. In particular, at $T \ll T_B$, the free-free opacities tabulated by Silant'ev & Yakovlev (1980) tend to

$$K_{\rm r}(B) \approx (23.2\,T/T_B)^2 K_{\rm r}(0) \simeq 2.2\,\bar{g}_{\rm eff}\,(Z/\mu_{\rm e}^2)\,\rho\,T_6^{-1.5}\,B_{12}^{-2}\ {\rm cm}^2/{\rm g}, \quad (35)$$

where $K_{\rm r}(0)$ is given by Eq. (12). This estimate may be used if only $T_6 \lesssim B_{12}$, $\chi \ll 1$, and the opacity is dominated by the free-free processes.

From Eqs. (2), (20), and (35) one sees immediately that the *radiative surface* in the strong magnetic fields, $B_{12} \gtrsim T_6$, is pushed to the higher densities, $\rho_{\rm s} \propto B$.

Caution is necessary however while using the scaling law (35). The strong magnetic field shifts the ionization equilibrium toward a lower degree of ionization, because of the increasing binding energies. Therefore, even if the plasma were fully ionized at some ρ and T in the absence of magnetic field, it may be only partially ionized at the same ρ and T when B is high. This increases the significance of the bound-bound and bound-free opacities and may result in a total radiative opacity considerably larger than that given by Eq. (35) (see, e.g., Potekhin *et al.* 1998).

Electron conductivities. Unified expressions and fitting formulae for thermal and electrical electron conductivities in a fully ionized degenerate plasma with arbitrary magnetic field have been obtained recently (Potekhin 1999). These conductivities undergo oscillations of the de Haas–van Alphen type at $\rho \gtrsim \rho_B$. At $B \gg 10^{10}$ G, the transport across the field is suppressed by orders of magnitude. This fact allows us to neglect $\kappa_\perp$ totally, which will be a good approximation everywhere except at a narrow stripe near the magnetic equator, where $\theta \approx \pi/2$.

This approximation, $\kappa \approx \kappa_\parallel \cos^2\theta$, holds despite the arguments by Heyl & Hernquist (1998) that $\kappa_\perp$ becomes non-negligible in the strongly quantizing regime at low density because the ratio $\kappa_\perp/\kappa_\parallel$ evaluated for strongly degenerate electrons increases without bound as $\chi \to 0$. However, the finite thermal width of the Fermi level (neglected by these authors) removes the divergency. At typical NS temperatures, the thermal averaging terminates the growth of $\kappa_\perp$ and moderates the decrease of $\kappa_\parallel$, before they become comparable. In Fig. 2, we plot by solid lines an example of the thermal conductivities calculated according to Potekhin (1999). For comparison,

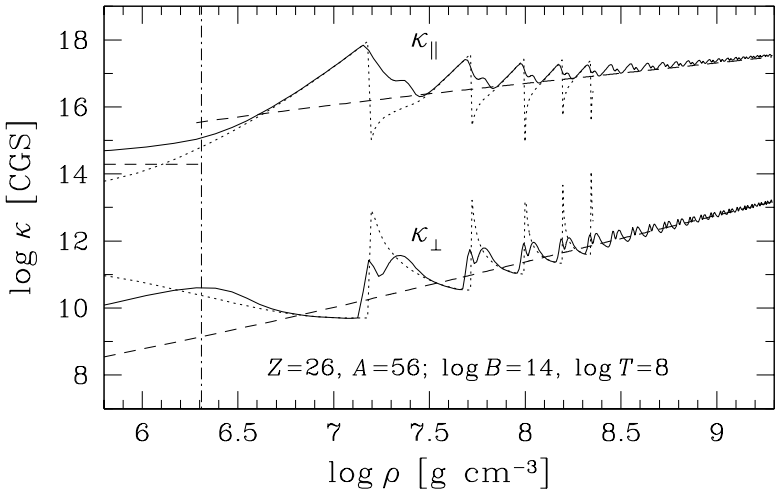

Figure 2. Longitudinal (∥) and transverse (⊥) thermal conductivities in the outer NS envelope composed of iron at $T = 10^8$ K and $B = 10^{14}$ G: comparison of accurate results (solid lines) with the classical approximation (dashed lines) and with the results without thermal averaging. The electrons are degenerate to the right of the vertical dot-dashed line, which corresponds to $T = T_{\rm F}$. The dashed horizontal line in the non-degenerate region shows the conductivity given by Eq. (14) with $F_Z/\Lambda = 1$.

the dotted curves display the conductivities which would have been obtained without thermal averaging. As the electrons become non-degenerate at low densities, the solid curve for $\kappa_\parallel$ is seen to level off. It tends to its non-degenerate value $\kappa_\parallel^{\rm nd}$ which is of the order of the non-magnetic value, Eq. (14), depending on density only logarithmically.

The dashed lines show the "classical" approximation where the quantizing nature of the field is neglected. For $\kappa_\parallel$, this approximation is close to the non-magnetic one. We can see that at high enough densities beyond the first oscillation, the classical approximation is good enough. At lower densities, the quantizing nature of the field must be taken into account. At $\rho < \rho_B$, the neglect of thermal averaging is justified as long as the electrons are degenerate. Then the longitudinal conductivity may be written as

$$\kappa_\parallel = \frac{k^2 T\,(m_{\rm e}^2 c^3 b)^2}{12\pi\hbar^3 Z e^4 n_{\rm e}}\,\frac{\chi^2}{2Q^\parallel} = \frac{2}{3}\,\frac{\kappa_0\,(1+\chi_0^2)\,\Lambda}{Q^\parallel}, \tag{36}$$

where κ_0 is the non-magnetic conductivity given by Eq. (13), in which χ must be replaced by χ_0, Λ is the non-magnetic Coulomb logarithm, and $Q^\parallel$ is a function of χ defined by Eq. (A9) in Potekhin (1999). In the liquid

regime (far enough from the solid phase boundary), the latter function reduces to the expression (Yakovlev 1984)

$$Q^{\parallel} = \xi^{-1} - \mathrm{e}^{\xi} E_1(\xi), \tag{37}$$

where $\xi = 2\chi^2/b + \frac{1}{2}(a_{\rm m} q_{\rm s})^2$, $q_{\rm s}$ is an effective Coulomb-screening wave number, and E_1 is the standard exponential integral. A simple order-of-magnitude estimate of $\kappa_{\parallel}$ in the degenerate Coulomb liquid can be obtained if we neglect $q_{\rm s}$ and the second term in Eq. (37). In this way we obtain

$$\kappa_{\parallel} \simeq (4/3)\,\kappa_0\,\Lambda(1+\chi_0^2)\,\chi^2/b \simeq 5\times 10^{15}\,Z^{-1}\,T_6\,\chi^3 \ \mathrm{erg/(cm\ s\ K)}. \tag{38}$$

As noted earlier, in the very strong fields considered here the onset of degeneracy is pushed into ever increasing densities as B increases. Therefore the turnover from radiative heat transfer to electron-conduction dominated transport may occur in the non-degenerate regime. In this case, Eq. (14) may be used to evaluate $\kappa_{\parallel}$.

3.3. CONSEQUENCES FOR THE HEAT TRANSPORT

We have seen that in strong magnetic fields there are several different regimes regulating the EOS and opacities. For the construction of an approximate analytic thermal profile it is sufficient to note that the non-magnetic expressions for the radiative opacity and *longitudinal* electron conductivity $\kappa_{\parallel}$ remain good approximations unless the field is strongly quantizing. Magnetic oscillations, which occur around the classical functions, will be smoothed out by integration while obtaining the thermal profile from Eq. (9); thus they are not too important.

When the field is strongly quantizing, the opacities are modified appreciably. However, in the degenerate part of NS ocean, which is of our prime interest here, the analytic expressions for $\kappa_{\parallel}$ can be again approximated as a power law, Eqs. (38) and (14). The same is true with respect to the extreme quantizing limit of radiative opacity, as follows from Eq. (35). In the non-degenerate regime, the magnetic field does not affect the EOS. In this case, we recover the solution (16) with new values of $\beta = -1.5$ and K_0, given by Eq. (35). Then

$$T_6 \approx 0.95\,(\bar{g}_{\rm eff}\,q)^{2/9}\,(\rho/\mu_{\rm e})^{4/9}\,B_{12}^{-4/9}, \tag{39}$$

with the same q as in Eq. (19). Thus the temperature is reduced (its profile becomes less steep) with increasing B as long as the field is strongly quantizing ($\rho < \rho_B$).

It is interesting to note that the value of the constant conductivity, Eq. (17) is independent of the magnetic field, while its numerical value is only slightly lowered as a result of the changed coefficient β.

Sensitivity strip. As we have seen, the sensitivity strip is placed near the turning point from radiative transport to electron conduction, defined by $K_{\rm r} = K_{\rm c}$. In a strongly quantizing field, using Eqs. (35) and (38), we have

$$\rho \approx 250\,\mu_{\rm e}\,\bar{g}_{\rm eff}^{-0.2}\,T_6^{0.7}\,|\cos\theta|^{-0.4} B_{12}\ \ {\rm g\,cm^{-3}} \tag{40}$$

instead of Eq. (23). With the temperature profile (39), we now obtain

$$T_{\rm t} \approx \frac{3.5\times10^7}{|\cos\theta|^{8/31}}\,\bar{g}_{\rm eff}^{6/31}\,q^{10/31}\ \ {\rm K}, \quad \frac{\rho_{\rm t}}{\mu_{\rm e}} \approx \frac{3\times10^3\,q^{7/31}\,B_{12}}{|\cos\theta|^{18/31}\,\bar{g}_{\rm eff}^{2/31}}\ {\rm g\,cm^{-3}}. \tag{41}$$

If, however, the electrons are non-degenerate along the turnover line, then $\kappa_\parallel$ is represented by Eq. (14) instead of (38). In this case, we obtain the turnover at

$$\rho \approx 52\,\sqrt{\Lambda/F_Z}\,\mu_e\,\bar{g}_{\rm eff}^{-1/2}\,T_6\,|\cos\theta|^{-1}\,B_{12}\ \ {\rm g\,cm^{-3}}. \tag{42}$$

Applying Eq. (39), we get

$$T_{\rm t} \approx \frac{2.2\times10^7}{|\cos\theta|^{0.8}}\left(\frac{\Lambda q}{F_Z}\right)^{0.4}{\rm K}, \quad \frac{\rho_{\rm t}}{\mu_{\rm e}} \approx \frac{1.1\times10^3\,q^{0.4}\,B_{12}}{|\cos\theta|^{1.8}\,\bar{g}_{\rm eff}^{0.5}}\left(\frac{\Lambda}{F_Z}\right)^{0.9}\ {\rm g\,cm^{-3}}.$$

Thus, in both cases (for degenerate and non-degenerate electrons) we have obtained similar dependences of the position of the turning point on the NS parameters. These dependences should be compared with Eq. (24). We see that $T_{\rm t}$ in both equations have similar values at $\theta = 0$, but in the magnetic field $T_{\rm t}$ increases with increasing θ. It is noteworthy that $T_{\rm t}$ is independent of B, while $\rho_{\rm t}$ grows linearly with B in the strongly quantizing field. From Eq. (31) we can evaluate the condition at which $\rho_{\rm t}$ lies in the region of strong magnetic quantization. Assuming that θ is not close to $\pi/2$ and neglecting factors about unity, we see that $\rho_{\rm t} < \rho_B$ for $B_{12} \gtrsim (Z\,T_{\rm e6}^4/g_{14})^{14/31}$, i.e., for the strong-field pulsars and magnetars.

Onset of degeneracy. Let us estimate the point at which the electrons become degenerate. For simplicity, let us assume that the electrons are non-relativistic. Taking into account Eqs. (3) and (34), we see that the condition $T = T_{\rm F}$ in the strongly quantizing magnetic field is equivalent to $\rho \approx 608\,\mu_{\rm e}\,\sqrt{T_6}\,B_{12}$. Then from Eq. (39) we obtain $\rho_{\rm d} \simeq 3700\,(\bar{g}_{\rm eff}\,q)^{1/7}\mu_{\rm e}B_{12}$. Thus, similar to the non-magnetic case, the switch between the regimes of photon and electron heat conduction occurs not far from the onset of degeneracy: $\rho_{\rm d} \sim \rho_{\rm t}$. Depending on θ, it can occur either in the non-degenerate domain (at $\theta \approx 0$) or in the degenerate domain (at $\theta \gtrsim 60^\circ$).

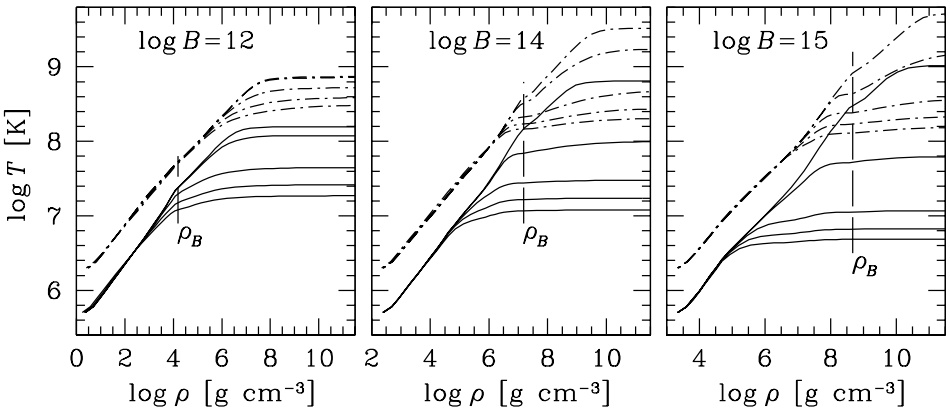

Figure 3. Temperature profiles through an iron envelope of a NS with $M = 1.4\,M_\odot$, $R = 10$ km, and with magnetic field $B = 10^{12}$ (left), 10^{14} (middle), or 10^{15} G (right panel). In every case, effective surface temperature was fixed to $T_\mathrm{e} = 5 \times 10^5$ K (solid lines) or 2×10^6 K (dot-dashed lines). Different lines of each bunch correspond to different values of $\cos\theta$: 1 (the lowest line of a bunch), 0.7, 0.4, 0.1, and 0 (the highest line).

Beyond the turning point. The integration beyond the turning point in order to obtain T_i can be done in the same way as in the non-magnetic case. However, since the turnover occurs in the strongly quantizing field, the integration path should be divided in two parts: below ρ_B, where Eq. (38) should be used for the conductivity, and above ρ_B, where one can use Eq. (25) with the right-hand side divided by $\cos^2\theta$. The result is similar to Eq. (27), but contains a profound dependence on the inclination angle: the thermal gradient grows rapidly as θ increases toward $\pi/2$.

This dependence is illustrated in Fig. 3, where we have shown several temperature profiles calculated numerically (Potekhin 2000). The curves start at the radiative surface, where $T = T_\mathrm{e}$, and end near the neutron drip point. The onset of the profound θ-dependence signals the turning point. According to our estimates above, this point is shifted to ever higher densities with increasing B. For the radiative boundary, the above-mentioned linear dependence $\rho_\mathrm{s} \propto B$ is confirmed. Another interesting effect is that T may continue to grow up to the bottom of the outer envelope, well beyond the "canonical" limiting density $\rho = 10^{10}$ g cm^{-3}.

4. Conclusions

In the preceding sections we have given a simplified analytic discussion of the neutron star outer envelope. It was possible in this simple picture to recover main features of more careful numerical calculations, such as the sensitivity of the temperature ratio $T_\mathrm{i}/T_\mathrm{e}$ to chemical constitution and the

general behavior of the (T, ρ) profile.

Magnetic fields have a strong influence on the radiative and conductive opacities in NS envelopes, as we have seen in the last section. It is remarkable though that in the region of the magnetic polar cap, in spite of the sharply reduced radiative opacities in the outer layers, the temperature ratios $T_{\rm t}/T_{\rm e}$, and $T_{\rm i}/T_{\rm e}$ are only mildly affected. The effect of the reduced opacity is partly counterbalanced by the increased mass of the radiative layer. Furthermore, when the magnetic field is inclined to the surface, the temperature gradient is increased because the electron conduction is efficient mainly along the field lines. Clearly more work is still necessary to fully analyze all these details.

The possibility of magnetars, or extremely highly magnetized NS, in our Galaxy has been highlighted by recent observations of soft gamma repeaters (Kouveliotou 1998, 1999; Thompson 2000) and the special class of anomalous X-ray pulsars (e.g., Mereghetti 2000). Understanding the role of high magnetic fields in the observable properties of such objects has thus become an important theoretical task. Recent observations of compact galactic objects further suggest rather small emission areas and high temperatures, which may be attributed to magnetars (e.g., Pavlov *et al.* 2000; Dar & de Rújula 2000). The presence of an accreted hydrogen layer on the magnetar's polar cap could allow for a rather sharp temperature contrast between the hot spot and the rest of the NS surface. This configuration has been invoked to interpret the observations in the case of the central compact object in the supernova remnant Cas A (Pavlov *et al.* 2000).

Acknowledgments. We thank D.G. Yakovlev for useful remarks. J.V. is deeply indebted to Vladimir Usov and Motty Milgrom for their generous hospitality and partial support from the Einstein Center for Theoretical Physics at the Weizmann Institute of Science; he also acknowledges partial support from EC grant ERB-FMRX-CT98-0195. A.Y.P. gratefully acknowledges generous hospitality of Gilles Chabrier at CRAL, Ecole Normale Supérieure de Lyon, and partial support from grants RFBR 99-02-18099 and INTAS 96-542.

References

Alpar, M.A., Cheng, K.S., & Pines, D. (1989). Vortex creep and the internal temperature of neutron stars, *Astrophys. J.* **346**, 823

Braginskiĭ, S.I. (1957). Transport phenomena in a plasma, *Zh. Eksp. Teor. Fiz.* **33**, 645

Blandford, R.D., & Hernquist, L. (1982). Magnetic susceptibility of a neutron star crust, *J. Phys. C: Solid State Phys.* **15**, 6233

Canuto, V., & Ventura, J. (1977). Quantizing magnetic fields in astrophysics, *Fundam. Cosm. Phys.* **2**, 203

Caraveo, P., Bignami, G. & Trümper, J. (1996). Radio-silent isolated neutron stars as a new astronomical reality, *Astron. & Astrophys. Rev.* **7**, 209

Chabrier, G. (1993). Quantum effects in dense Coulombic matter – Application to the cooling of white dwarfs, *Astrophys. J.* **414**, 695

Chabrier, G., & Potekhin, A.Y. (1998). Equation of state of fully ionized electron-ion plasmas, *Phys. Rev. E* **58**, 4941

Chiu, H.Y., & Salpeter, E.E. (1964). Surface X-ray emission from neutron stars, *Phys. Rev. Lett.* **12**, 413

Cox, J.P., & Giuli, R.T. (1968). *Principles of Stellar Structure* (Gordon and Breach, New York)

Dar, A. & de Rújula, A. (2000). SGRs and AXPs: Magnetars or young quark stars? astro-ph/0002014

Gudmundsson, E.H., Pethick, C.J., & Epstein, R.I. (1983). Structure of neutron star envelopes, *Astrophys. J.* **272**, 286 (GPE)

Halpern, J.P., & Ruderman, M. (1993). Soft X-ray properties of the Geminga pulsar, *Astrophys. J.* **415**, 286

Hernquist, L., & Applegate, J.H. (1984). Analytical models of neutron star envelopes, *Astrophys. J.* **287**, 244 (HA84)

Heyl, J.S., & Hernquist, L. (1998). Almost analytic models of ultramagnetized neutron star envelopes, *Mon. Not. R. Astron. Soc.* **300**, 599

Iglesias, C.A., & Rogers, F.J. (1996). Updated OPAL opacities, *Astrophys. J.* **464**, 943; `http://www-phys.llnl.gov/V_Div/OPAL/opal.html`

Kouveliotou, C. *et al.* (1998). An X-ray pulsar with a superstrong magnetic field in the soft gamma-ray repeater SGR 1806–20, *Nature* **393**, 235

Kouveliotou, C. *et al.* (1999). Discovery of a magnetar associated with the soft gamma repeater SGR 1900+14, *Astrophys. J.* **510**, L115

Lai, D., & Salpeter, E.E. (1997). Hydrogen phases on the surface of a strongly magnetized neutron star, *Astrophys. J.* **491**, 270

Mereghetti S. (2000). The anomalous X-ray pulsars, this volume

Mészáros, P. (1992). *High Energy Radiation from Magnetized Neutron Stars* (U. of Chicago Press, Chicago)

Miller, M.C., & Neuhauser, D. (1991). Atoms in very strong magnetic fields, *Mon. Not. R. Astron. Soc.* **253**, 107

Page, D. (1997). Fast cooling of neutron stars, *Astrophys. J.* **479**, L43

Page, D., & Sarmiento, A. (1996). Surface temperature of a magnetized neutron star and interpretation of the *ROSAT* data. II, *Astrophys. J.* **473**, 1067

Pavlov, G.G., Shibanov, Yu.A., Zavlin, V.E., & Meyer, R.D. (1995). Neutron star atmospheres, in: M.A. Alpar, Ü. Kiziloğlu, & J. van Paradijs (eds.), *The Lives of the Neutron Stars*, NATO ASI Ser. C **450** (Kluwer, Dordrecht) p. 71

Pavlov, G.G., Zavlin, V.E., Aschenbach, B., Trümper, J., & Sanwal, D. (2000). The compact central object of Cassiopeia A: a neutron star with hot polar caps or a black hole? *Astrophys. J.* **531**, L53

Pethick, C.J. (1992). Cooling of neutron stars, *Rev. Mod. Phys.* **84**, 1133

Potekhin, A.Y. (1999). Electron conduction in magnetized neutron star envelopes, *Astron. & Astrophys.* **351**, 787

Potekhin, A.Y. (2000). Heat and charge transport in envelopes of weakly and strongly magnetized neutron stars, in: M. Kramer, N. Wex, & R. Wielebinski

(eds.), *Pulsar Astronomy – 2000 and beyond*, ASP Conf. Ser. **202**, 621

Potekhin, A.Y., Chabrier, G., & Yakovlev, D.G. (1997). Internal temperatures and cooling of neutron stars with accreted envelopes, *Astron. & Astrophys.* **323**, 415 (PCY)

Potekhin, A.Y., Shibanov, Yu.A., & Ventura, J. (1998). Equation of state and opacities for hydrogen atmospheres of strongly magnetized cooling neutron stars, in: N. Shibazaki, N. Kawai, S. Shibata, & T. Kifune (eds.), *Neutron Stars and Pulsars* (Universal Academy Press, Tokyo) p. 161

Potekhin, A.Y, Baiko, D.A., Haensel, P., & Yakovlev, D.G. (1999a). Transport properties of degenerate electrons in neutron star envelopes and white dwarf cores, *Astron. & Astrophys.* **346**, 345

Potekhin, A.Y., Chabrier, G., & Shibanov, Yu.A. (1999b). Partially ionized hydrogen plasma in strong magnetic fields, *Phys. Rev. E* **60**, 2193

Rajagopal, M., Romani, R., & Miller, M.C. (1997). Magnetized iron atmospheres for neutron stars, *Astrophys. J.* **479**, 347

Reisenegger, A. (1997). Constraining dense matter superfluidity through thermal emission from millisecond pulsars, *Astrophys. J.* **485**, 313

Romani, R.W. (1987). Model atmospheres for cooling neutron stars, *Astrophys. J.* **313**, 718

Ruderman, M.A. (1971). Matter in superstrong magnetic fields: the surface of a neutron star, *Phys. Rev. Lett.* **27**, 1306

Shapiro, S.L., & Teukolski, S.A. (1983). *Black Holes, White Dwarfs, and Neutron Stars: The Physics of Compact Objects* (Wiley, New York) (ST83)

Shibanov, Yu.A., Potekhin, A.Y., Yakovlev, D.G., & Zavlin, V.E. (1998). Evolution of thermal structure and radiation spectrum of cooling neutron stars, in: R. Buccheri, J. van Paradijs, & M.A. Alpar (eds.), *The Many Faces of Neutron Stars* (Kluwer, Dordrecht) p. 553

Silant'ev, N.A., & Yakovlev, D.G. (1980). Radiative heat transfer in surface layers of neutron stars with a magnetic field, *Astrophys. Space Sci.* **71**, 45

Thompson, C. (2000). The soft gamma repeaters, this volume

Thorne, K.S. (1977). The relativistic equations of stellar structure and evolution, *Astrophys. J.* **212**, 825

Trümper, J., & Becker, W. (1997). X-ray emission from isolated neutron stars, *Adv. Space Res.* **21**, 203

Tsuruta, S. (1998). Thermal properties and detectability of neutron stars. II. Thermal evolution of rotation-powered neutron stars, *Phys. Rep.* **292**, 1

Urpin, V.A., & Yakovlev, D.G. (1980). On temperature growth inside neutron stars, *Astrophysics* **15**, 429

Ventura, J. (1989). Radiation from cooling neutron stars, in: H. Ögelman & E.P.J. van den Heuvel (eds.), *Timing Neutron Stars* (Kluwer, Dordrecht) p. 491

Yakovlev, D.G. (1984). Transport properties of the degenerate electron gas of neutron stars along the quantizing magnetic field, *Astrophys. Space Sci.* **98**, 37

Yakovlev, D.G., & Kaminker, A.D. (1994). Neutron star crusts with magnetic fields, in: G. Chabrier & E. Schatzman (eds.), *The Equation of State in Astrophysics*, Proc. IAU Coll. 147 (Cambridge U. Press, Cambridge, UK) p. 214

Yakovlev, D.G., & Urpin, V.A. (1980). Thermal and electrical conductivity in white dwarfs and neutron stars, *Sov. Astron.* **24**, 303

Yakovlev, D.G., Levenfish, K.P., & Shibanov, Yu.A. (1999). Cooling neutron stars and superfluidity in their interior, *Physics–Uspekhi* **42**, 737